Nature Environment and Pollution Technology
An International Quarterly Scientific Journal

| ISSN: 0972-6268 | Vol. 15 | No. 1 | pp. 1-10 | 2016 |
|---|---|---|---|---|

Original Research Paper

# Numerical Investigation of Ash Particles Deposition and Distribution in a Refining and Chemical Wastewater Incineration Equipment

**Lin Mu*, Qinggang Qiu*, Jianbiao Chen*, Hongchao Yin*†, Aimin Li** and Xiao Chi*****

*Key Laboratory of Ocean Energy Utilization and Energy Conservation of Ministry of Education, School of Energy and Power Engineering, Dalian University of Technology 116023, Dalian, China

**Key Laboratory of Industrial Ecology and Environmental Engineering (MOE), School of Environmental Science and Technology, Dalian University of Technology 116023, Dalian, China

***Heat/Electric Power Engineering Design Deptt. NORINDAR International (Group) Ltd., 050011, Shijiazhuang, China

†Corresponding author: Hongchao Yin

**Nat. Env. & Poll. Tech.**
**Website: www.neptjournal.com**

*Received:* 25-06-2015
*Accepted:* 15-08-2015

**Key Words:**
Numerical simulation
Gas-particle two-phase flow
Impaction efficiency
Ash particles deposition
Incineration equipment

## ABSTRACT

In this paper, numerical investigation has been performed to predict ash particles impaction and distribution tendencies in a heat recovery steam generator (HRSG) of an industrial refining and chemical wastewater incineration plant. A two-dimensional mathematical model with a six-row staggered arrangement has been built in order to study gas-particle two-phase flow in the HRSG, and the effects of ash particle size, flue gas velocity, longitudinal tube pitch and spanwise tube pitch on ash particle impaction efficiency were investigated. Overall, all parameters played important roles in ash particle impaction performance except longitudinal tube pitch. The results showed that large particles mainly impacted on the windward side of the first two rows of tubes, while small particles impacted on both windward and leeward sides forming a uniform distribution. Enhancing the particle size and flue gas velocity contributed more ash particles to impact on the heat transfer surfaces, moreover, 20 μm particles were much more sensitive to fluid velocity compared with 0.2 μm particles. As for spanwise tube pitch, the results indicated that it had an obvious effect on decreasing the impaction efficiency with an increase of spanwise tube pitch, while with the increase of longitudinal tube pitch, the impaction efficiency declined slightly.

## INTRODUCTION

Incineration is a well-established method which was often applied to dispose the industrial organic wastewater with high toxicity, poor bio-degradability and complex composition, making the poisonous and harmful constituent degraded completely (Mu et al. 2012a). Meanwhile, the waste heat generated during the thermal treatment process can be recovered by heat recovery steam generator (HRSG) for the purpose of energy saving and environmental protection. However, during the thermal degradation process a great amount of incombustible inorganic matter can be released and transformed to ash forming species, especially ash particles. When these troublesome ash particles are carried by flue gas into heat recovery section, they tend to deposit on the surfaces of heat transfer tubes, leading to some serious ash-related problems, such as fouling and slagging (Ma et al. 2014, Mu et al. 2015). As the time scale increases, ranging from minutes to days, continuous accumulated ash deposits can form fly ash bridge and/or clinker, which aggravate heat transfer efficiency and high temperature corrosion significantly, further resulting in unscheduled shutdown (Zbogar et al. 2005).

Ash particle transport and deposition is a sophisticated combination of physical and chemical processes, and many factors such as particle morphological properties, chemical compositions, turbulent dispersion and particle interactions, fluid or particle temperature, impact/adhesion/rebound mechanisms are involved (Venturini et al. 2012). It is generally agreed that the relative important transport mechanisms related to the deposition and distribution of ash particles in a typical combustion or incineration environment are: inertial impaction, eddy diffusion and deposition, thermophoretic deposition, condensation, and chemical reaction. In some special cases, other deposition mechanisms such as electrostatic interactions and photophoresis are contained (Zbogar et al. 2009, Mu et al. 2012b). Among these normal transport mechanisms, inertial impaction is expected to be the dominant mechanism, at least for large particles (>10 μm), however, for ash particles in micron or sub-micron sizes, eddy diffusion and thermophoretic deposition control the ash particle trajectories along the flue gas flow as well as the fates of ash particles near the walls (Han et al. 2014).

As the development of Computational Fluid Dynamics (CFD), the motion of ash particles as well as interaction

with the heat transfer surfaces in a boiler or HRSG has been efficiently predicted by solving gas-particle (or droplet) two-phase flow. However, modeling of the particle-wall impact process in conjunction with gas-particle (or droplet) two-phase flow remains difficult. When the flue-ash particles collided with a heat transfer surface, the particles might adhere to the surface if the incident velocity was below the critical sticking velocity and might rebound or remove other deposited particles if the incident velocity was above the critical sticking velocity (Abd-Elhady et al. 2006). Nevertheless, a simulation model built up on a basis of actual equipment gives important guidance to improve understanding how ash deposition and distribution affects the boiler or HRSG performance. Meanwhile, CFD-based deposition model also makes it possible to investigate the effects of individual deposition phenomena in isolation or in combination with others (Sandberg et al. 2011). Many attempts have therefore been made on a basis of numerical modelling to study the interaction between the ash particles with heat transfer surfaces, in order to minimize ash-related problems and improve heat transfer efficiency (Zhou et al. 2007, Fang et al. 2010). Lee et al. (2014) developed a numerical deposition model based on the force balance equations such as elastic rebound, van der Waals and gravity, and the results indicated that the ash particles with small size and low velocity had high deposition rates due to strong adhesion force. By applying the user defined functions (UDFs) of dynamic mesh, Waclawiak & Kalisz (2012) proposed a novel deposition model to predict the fouling process in a macro scale, and further evaluated the shapes of powdery deposition and heat transfer features of fouled tube banks. Han et al. (2014) examined the effects of particle size, flow velocity, tube geometries as well as spanwise and longitudinal tube pitches on the ash particle deposition and rebounding. An integrated particulate deposition model has been proposed by Pan et al. (2011), to numerically predict particle deposition and the fouling removal process, and internal micro-structure, surface morphology and mechanical properties of pre-deposited surface were taken into consideration.

The motion of ash particles and the impaction processes of ash particles on the heat transfer surfaces are the prerequisite to motivate ash-related problems. Consequently, it is of great importance to investigate impaction processes of ash particles on the surfaces of heat transfer tubes and quantify the impaction efficiency of ash particles. Therefore, in this paper, a commercial CFD code FLUENT is implemented to solve particle trajectories and the particle destinies (sticking or rebounding) after impacting on the heat transfer surfaces. A diluted Eulerian-Lagrangian gas-solid two phase model is applied to simulate turbulent flow field, the effects of particle size, flow velocity, longitudinal tube pitch and spanwise tube pitch on ash particle impaction and distribution characteristics are investigated.

## PHYSICAL MODEL AND NUMERICAL APPROACH

**Physical model:** The studied HRSG in this paper is a horizontal corner tube boiler which is applied in Sinopec Shijiazhuang Chemical Fiber Co., Ltd., Hebei, China. According to some useful conclusions (Han et al. 2014, Tomeczek & Waclawiak 2009), the flow state of flue gas, after passing six rows of tube bundle, is prone to be stable, therefore, for the purpose of analyzing ash particle impaction and distribution on the different positions of tube surfaces conveniently, a simplified 2D computational model with six-row tube bundle is adopted, as shown in Fig. 1(a). Each tube has the outer diameter and wall thickness of 51 mm and 3 mm, respectively. Fig. 1(b) is the computational grid and boundary conditions used for the simulation, which will be discussed later in detail.

**Modelling of continuous phase:** In general, the Euler-Lagrangian approach is applied to solve the diluted gas-solid two phase problem. The continuous phase is solved by using the time-averaged Navier-Stokes equations, while the dispersed phase is solved by tracking a large number of particles through the calculated flow field, and the exchange of momentum, mass, and energy between the continuous phase and the dispersed phase is considered.

A proper representation of the primary flow is crucial for adequate prediction of impaction and distribution characteristics of ash particles under different operating conditions. In this study, the fluid, i.e. flue gas is considered to be in-compressible, therefore, the physical properties of the flue gas is local temperature dependent. The simulation of flue gas turbulent flow is carried out by using standard k-ε model with the enhanced wall functions. Han et al. (2014) pointed out that enhanced wall functions have some advantages such as precision and accuracy in evaluating the heat transfer and

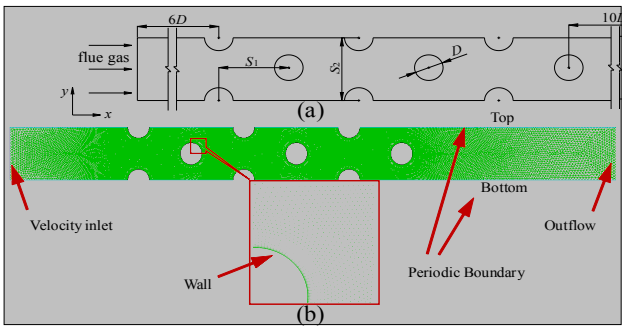


Fig. 1: Schematic diagram of tube bank arrangement in the HRSG: (a) the simplified six-row tube bundle, and (b) computational grid and boundary conditions used for the simulation.

flow conditions near wall, if under acceptable computational consumption. The kinetic energy of the turbulent $k$ and its dissipation rate ε of the standard $k$-ε model used in this paper is governed by the separate transport equations:

$k$–equation:

$$\frac{\partial}{\partial t}(\rho k)+\frac{\partial}{\partial x_i}(\rho k u_i)=\frac{\partial}{\partial x_j}\left[\left(\mu+\frac{\mu_t}{\sigma_k}\right)\frac{\partial k}{\partial x_j}\right]+G_k+G_b-\rho\varepsilon-Y_M \quad ...(1)$$

ε–equation:

$$\frac{\partial}{\partial t}(\rho \varepsilon)+\frac{\partial}{\partial x_i}(\rho \varepsilon u_i)=\frac{\partial}{\partial x_j}\left[\left(\mu+\frac{\mu_t}{\sigma_\varepsilon}\right)\frac{\partial \varepsilon}{\partial x_j}\right]+C_{1\varepsilon}\frac{\varepsilon}{k}(G_k+C_{3\varepsilon}G_b)-C_{2\varepsilon}\rho\frac{\varepsilon^2}{k} \quad ...(2)$$

Where, $G_k$ and $G_b$ are the generation of turbulence kinetic energy due to the mean velocity gradients and buoyancy, respectively, $Y_M$ is the contribution of the fluctuating dilatation in compressible turbulence to the overall dissipation rate. The model constants are listed as follows: $C_1\varepsilon$=1.44, $C_{2\varepsilon}$=1.92, $C_\mu$=0.09, $\sigma_k$=1.0 and $\sigma_\varepsilon$=1.3.

**Modelling of discrete phase:** The stochastic Lagrangian approach is used to track ash particle trajectories in the particle-laden flue gas flow. In this study, it is assumed that the modelled ash particles are spherical, non-reacting and non-rotating. Then in a Lagrangian reference frame, the trajectory of an ash particle is described numerically by a set of ordinary differential equations, taking into consideration the possible forces, the drag force, the Brownian force, Saffman's lift force and the thermophoretic force, acting upon it. Then the particle motion equation in Cartesian coordinates is given as:

$$\frac{\mathrm{d}u_\mathrm{p}}{\mathrm{d}t}=F_\mathrm{D}(u-u_\mathrm{p})+F_\mathrm{TH}+F_\mathrm{B}+F_\mathrm{L} \quad ...(3)$$

Where, $F_\mathrm{D}(u–u_\mathrm{p})$, $F_\mathrm{B}$, $F_\mathrm{L}$ and $F_\mathrm{TH}$ are the drag force, Brownian force, Saffman's lift force and thermosphoretic force, respectively. For the drag force $F_\mathrm{D}(u\text{-}u_\mathrm{p})$, $u$ and $u_\mathrm{p}$ are the continuous phase velocity and the particle velocity, respectively, and $F_\mathrm{D}$ can be calculated as follows:

$$F_\mathrm{D}=\left(\frac{18\mu}{\rho_\mathrm{p}d_\mathrm{p}^2C_\mathrm{C}}\right)C_\mathrm{D}\left(\frac{\mathrm{Re}_\mathrm{p}}{24}\right) \quad ...(4)$$

Where, $\mu$, $p$ and $d_\mathrm{p}$ are the molecular viscosity of the continuous phase, the continuous phase density, the particle density, respectively. $\mathrm{Re}_\mathrm{p}$ is the relative Reynolds number and given as $\mathrm{Re_p}=\rho d_\mathrm{p}|u_\mathrm{p}–u|/\mu$. $C_\mathrm{D}$ is the drag coefficient as a function of $\mathrm{Re}_\mathrm{p}$ according to (Li & Ahmadi 1992):

$$C_\mathrm{D}=\frac{24}{\mathrm{Re}_\mathrm{p}}\frac{1}{C_\mathrm{C}} \qquad \text{for } \mathrm{Re_p}<1,$$

$$C_\mathrm{D}=\frac{24}{\mathrm{Re}_\mathrm{p}}\left(1+0.15\mathrm{Re}_\mathrm{p}^{0.687}\right) \qquad \text{for } 1<\mathrm{Re_p}<1000,$$

$$C_\mathrm{D}=0.44 \qquad \text{for } \mathrm{Re_p}>1000 \quad ...(5)$$

$C_\mathrm{C}$ is the Cunningham slip correction factor for rarefied gas effects and defined as (Guha 2008):

$$C_\mathrm{C}=1+\mathrm{Kn}\left(1.257+0.4e^{-\frac{1.1}{\mathrm{Kn}}}\right) \quad ...(6)$$

Where, $\mathrm{Kn}=2\lambda/d_p$ is the Knudsen number, λ is the molecular mean free path. For the sub-micron and micron particles, the mean free path is of the same order as particle size and the Cunningham slip correction factor will become important. As to the thermophoretic force, a modified thermophoresis force equation which was developed by Li & Ahmadi (1992) by adjusting its amplitude and some parameters was applied here:

$$F_\mathrm{TH}=1.15\frac{\mathrm{Kn}\cdot\left[1-e^{\left(-\frac{\alpha}{\mathrm{Kn}}\right)}\right]\cdot\left(\frac{4}{3\pi}\varphi\pi_1\mathrm{Kn}\right)^{\frac{1}{2}}\frac{k_\mathrm{B}}{d_\mathrm{m}^2}\nabla T d_\mathrm{p}^2}{4\sqrt{2}\alpha\left(1+\frac{\pi_1}{2}Kn\right)} \quad ...(7)$$

with

$$\alpha=0.22\left[\frac{\frac{\pi}{6}\varphi}{1+\frac{\pi_1}{2}\mathrm{Kn}}\right]^{\frac{1}{2}},\ \varphi=0.25(9\gamma-5)\frac{c_\mathrm{v}}{R_\mathrm{g}} \quad \text{and}$$

$$\pi_1=0.18\frac{\frac{36}{\pi}}{(2-S_\mathrm{n}+S_\mathrm{t})\frac{4}{\pi}+S_\mathrm{n}} \quad ...(8)$$

Where, $d_m$ is the molecular diameter, $k_\mathrm{B}=1.3806505\times10^{-23}$ J/K is the Boltzmann constant, $c_\mathrm{v}=718+0.1167p_\mathrm{p}$ J/kg·K is the constant volume specific heat, $R_\mathrm{g}$= 8.314 kJ/kmol·K is the gas constant and γ=1.4 is the specific heat ratio for the diatomic gas. $S_\mathrm{n}$ and $S_\mathrm{t}$ are the normal and tangential momentum accommodation coefficients, respectively, and when $S_\mathrm{n}=S_\mathrm{t}=1$, $\pi_1=0.5816$.

The turbulent dispersion of the particles in the continuous phase is predicted using the discrete random walk (DRW) model. Then the particle trajectories are calculated integrating the trajectory equation for individual particles, using the instantaneous value of the fluctuating gas flow velocity, $\bar{u}+u'$. The value of $u'$ is a Gaussian distributed random velocity fluctuation during the lifetime of the turbulent eddy, $u'=\zeta(\overline{u'^2})^{0.5}$, ζ and $(\overline{u'^2})^{0.5}$ are the normally distributed random number and the local root-mean-square velocity fluctuations, respectively. Since the discrete phase particles may dampen or produce turbulent eddies, the two-way coupling method is applied to consider the effects between the discrete phase and the continuous phase, while the effect of particle-particle interaction is ignored in the model.

According to Mu et al. (2012a), ash particles studied,

show a continuous but the typical bimodal distribution, therefore the continuous variation of the ash particle size distribution is simplified, as introduced by Zhou et al. (2007), in order to evaluate the deposition distribution characteristics of ash particles in specified sizes. As shown in Fig. 2, two peak values of ash particle diameters, 0.2 μm and 20 μm are adopted as a simplified description to perform ash particle size distribution with the flow rates of 0.002 kg/s and 0.0009 kg/s, respectively.

**Probability model of particle impaction:** Many factors, such as particle size, tube arrangement, flue gas velocity, physical properties of the ash particles and heat exchange tube wall, etc., have comprehensive influence on the deposition and distribution of ash particles on the heat transfer tube surfaces. Impaction process between particles and surfaces is precondition of ash deposition and subsequent sticking or shedding. Avoiding or mitigation of impaction through controlling physical or operation parameters and optimizing design is an effective method to minimize the ash related problems. Deposition efficiency of ash particles, $\eta_{deposit}$ can be calculated as follows:

$$\eta_{deposit} = \eta_{impact} \times \eta_{stick} = \frac{Q_{impact}}{Q_{total}} \times \eta_{stick} \quad ...(9)$$

where, $\eta_{impact}$ and $\eta_{stick}$ are the impaction efficiency and the sticking efficiency of ash particles, $Q_{impact}$ and $Q_{total}$ are the mass flow of particles impacting on the heat transfer tube surfaces and the total mass flow of particles entering the computational domain along with flue gas. In this study we just focus on the effects of particle size, flow velocity, longitudinal and spanwise tube pitches on ash particle impaction and distribution characteristics, therefore it is assumed that all the particles impacting on the surfaces can stick to the surface, that is to say, $\eta_{stick}$=1.

## MODEL SOLUTION

**Solution methods and boundary conditions:** In order to ensure the inlet uniformity, the computational domain is extended upstream for a distance of six times the diameter of heat transfer tubes in the entrance section, while at the exit; the domain is extended downstream for a distance of ten times the diameter of heat transfer tubes, as shown in Fig. 1(a). Four boundary conditions are included in the computational domain, and they are velocity inlet, outflow, wall and periodic boundary conditions (top and bottom). Under the design operating conditions the flue gas velocity and temperature at the entrance are 12 m/s and 1123 K, respectively, while normal velocity is 0. Non-slip boundary condition of velocity is adopted at the wall surface with a constant temperature of 456 K.

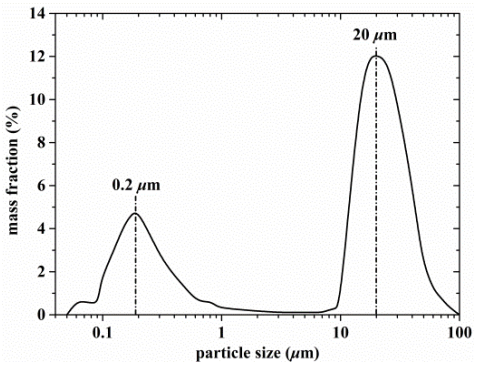


Fig. 2: Size distribution of ash particles showing a typical bimodal characteristics.

The DO (Discrete Ordinates) radiative heat transfer model combined with WSGG (Weighted-Sum-of-Grey-Gases) model is applied to solve radiative heat transfer equation and radiation characteristic of flue gas, respectively. SIMPLE (Semi-Implicit Method for Pressure-Linked Equations) semi-implicit iterative method is adopted to couple the velocity and pressure in order to satisfy continuity. As to turbulent kinetic energy and pressure evaluation and discretization, the second-order QUICK and the PRESTO schemes are used, while for other terms, the first-order unwind is used. The convergence criteria for all the parameters are achieved when the iteration residuals are reduced to 4 orders of magnitude. The numerical calculation is divided into two stages. In the first stage, continuum field of the flue gas is evaluated, and then the ash particles are added at the entrance with convergence of continuous phase calculation. UDFs (User-defined functions) are compiled and loaded to FLUENT equation solver to calculate the modified thermophoretic force acting upon the ash particles and impaction processes between particles and surfaces.

**Mesh generation and independence validation:** As shown in Fig. 1(b), unstructured grid and boundary layer mesh refinement techniques are both used. Compared to structured grid, unstructured grid possesses stronger geometric adaptability, while boundary layer mesh refinement near the wall surfaces can guarantee that $y^+$ value in the boundary layer is approximately equal to 1 (Weber et al. 2013). Properly sparse grids away from the wall are beneficial to reduce calculation cost. Grid-dependent tests have been performed and different computational meshes of 32896, 53624 and 85613 cells are tested. The results, as shown in Fig. 3, indicate that no significant difference is found between using 53624 and 85613 meshes, therefore, 53624 computational meshes are used in the present study to obtain the predicted results.

**Model validation:** In order to validate the reliability of the computational model and numerical method, Zhukauskas correlation is used. In this, a set of correlations suitable for

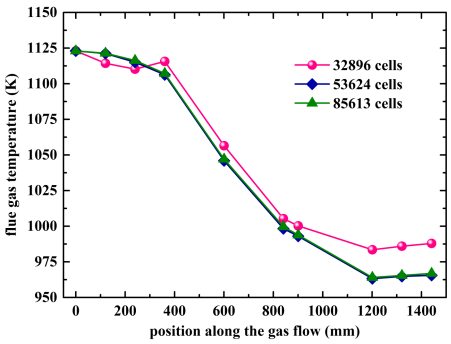


Fig. 3: Mesh independent verification.

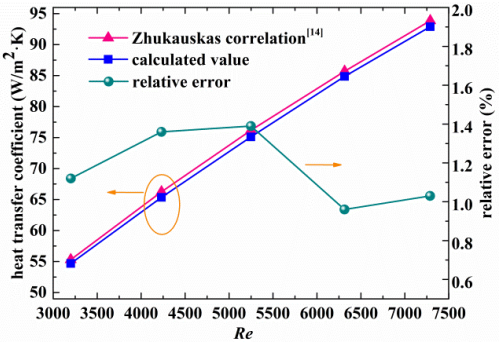


Fig. 4: Comparison of calculated and measured heat transfer coefficient for different Re.

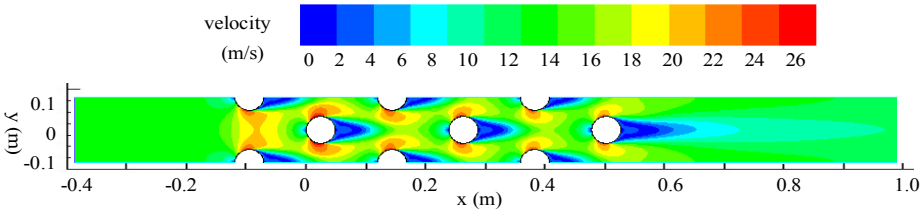


Fig. 5: Velocity contour of continuous phase.

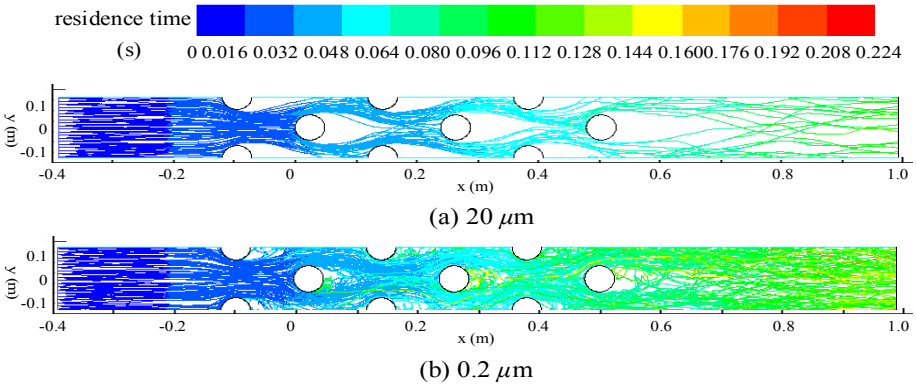


Fig. 6: Trajectories of ash particles with different sizes: (a) 20 μm and (b) 0.2 μm.

calculation of surface heat transfer coefficient from tube banks in crossflow at different Reynolds numbers over wide range of Prandtl number are summarized (Zhukauskas 1987). In this work, five different initial velocities of flue gas (6, 8, 10, 12 and 14 m/s) are carried out in order to study the effects of initial velocities on the ash particle impaction and distribution. And for the staggered tube bundle whose number of tube rows is more than 16, the correlation of mean surface heat transfer coefficient can be calculated by Nusselt number Nu as follows:

$$\mathrm{Nu} = 0.35(S_2 / S_1)^{0.2}\,\mathrm{Re}_f^{0.6}\,\mathrm{Pr}_f^{0.36}(\mathrm{Pr}_f / \mathrm{Pr}_w)^{0.25} \qquad ...(10)$$

Where, $S_1$ and $S_2$ are the spanwise tube pitch and longitudinal tube pitch, respectively. $\mathrm{Re}_f$ is the Reynolds number of flue gas, and evaluated by the qualitative temperature (which is equal to the average value of the flue gas temperatures at the entrance and at the exit of the computational domain) and the maximum flue gas velocity at the minimum cross section. Therefore, according to the initial physical parameters (such as flue gas temperature, density and viscosity) and five different pre-defined flue gas velocity, the Reynolds number of the flue gas ranges from 3200 to 7287. $\mathrm{Pr}_f$ and $\mathrm{Pr}_w$ are the Planck numbers characterized by the mainstream temperature and the wall surface temperature, respectively.

When the number of tube bundle is not more than 16, the correlation of the mean surface heat transfer coefficient should be multiplied by a correction coefficient of $\varepsilon_n$=0.942. Fig. 4 illustrates the comparison of numerically predicted heat transfer coefficients (calculated values) with the corresponding values established by Zhukaukas correlation. And the results show that the maximum relative error is 1.39% and the mean relative error is 1.17%, indicating the acceptable agreement.

## RESULTS AND DISCUSSION

In this section, the basic flow characteristics of flue gas in cross flow with 6-row tube bundle are discussed first, then the impaction processes between the ash particles and heat transfer tube surfaces are studied. The effects of ash particle size, flue gas velocity, spanwise tube pitch and longitudinal tube pitch are analyzed in detail. During the following numerical studies, the studies are always conducted veering a single parameter (i.e. ash particle size, flue gas velocity, spanwise tube pitch or longitudinal tube pitch), while all the other parameters are kept the same.

**The flue gas flow characteristics and ash particle trajectories:** The impaction processes between the ash particles and heat transfer surfaces are mainly affected by the flow features of flue gas which can be seen in Fig. 5. As illustrated in Fig. 5, flue gas velocity increases to a certain extent because of the decreasing of circulation section area between heat exchange tube bundles. The maximum velocity may reach 26 m/s. In addition, vortex flow fields shedding from aerodynamical bodies (i.e. heat transfer tubes) are found on the leeward sides to form wake vortices.

Fig. 6 shows the trajectories of ash particles with different sizes. As shown in Fig. 6(a), 20 μm ash particles have greater momentum, thus most of these large particles can travel along their own trajectories, and then impact on the windward sides of heat transfer tubes. While the momentum of 0.2 μm ash particles is much more lower than that of large particles. Some of them can follow with the flow of flue gas, and then be captured by the wake vortices on the leeward sides of heat transfer tubes, as shown in Fig. 6(b). Therefore, impaction of 0.2 μm ash particles may occur on the whole range of the heat transfer tubes, implying the impaction of ash particles can form a uniform distribution around the heat transfer surfaces, and the residence time in the computational domain is also longer than that of large particles.

**Effects of particle size on impaction process:** In order to study the effects of ash particle sizes on the impaction process, five different particle sizes are selected according to the typical bimodal distribution of particle sizes (see Fig. 2), and they are 0.2, 5, 20, 60 and 100 μm; other parameters are kept the same.

The impaction tendencies (characterized by impaction efficiency) of ash particles with different sizes on both windward and leeward sides of heat transfer tubes are illustrated in Fig. 7(a) and (b), respectively. As can be seen in Fig. 7(a), impaction processes of large particles ($d_p$=20, 60, 100 μm) and surfaces mainly take place on the windward sides of the first two rows of tubes, while the impaction efficiency of large particles on the leeward side is prone to be zero. The main reason is that, the inertial impaction is one of the most important transport mechanisms, controlling the large particles, especially larger than 10 μm (Han et al. 2014). Therefore, the large particles with great momentum are not as efficiently affected by flue gas flow, and likely to keep the existing trajectories to move forward and penetrate the boundary layer near the wall with enough normal momentum. As a result, they can impact on the surfaces of heat transfer tubes when the flue gas flow around the heat transfer tubes.

On the contrary, impaction of small particles ($d_p$=0.2, 5 μm) show a relatively uneven distribution over the whole surfaces of heat transfer tubes. Also it can be seen in Fig. 7(b), the impaction efficiency of ash particles on the leeward sides enhances firstly and then weakens with the increasing ash particle size. It is because that, transport-impaction control mechanisms such as eddy diffusion, thermophoresis and even Brownian motion effect have remarkable influences on the small particles (<10 μm), whose movements indicate more significant randomness around the surfaces of heat transfer tubes along the gas flow direction, showing a relatively average distribution, not only on an individual heat transfer tube, but also over the whole heat transfer tubes in the computational domain. Overall, small particles with less momentum can be easily captured by the wake vortices on the leeward sides of tubes and then follow downstream with the wake vortices shed from the front row tubes. While with the increase of the ash particle size, the ash particles attracted by the wake vortices decreases, leading to a reduction in impaction efficiency on the leeward sides. This further provides evidence that inertial transport-impaction mechanism, which mainly controls the ash particles with large sizes, is the dominant factor for forming ash deposits on the heat transfer surfaces. The results of impaction distribution and total impaction efficiency with different particle sizes obtained in this study, as shown in Fig. 7(c), have an acceptable agreement with the findings suggested by Zhou et al. (2007) and Haugen et al. (2013).

**Effects of flue gas velocity on impaction process:** As mentioned above, the inlet velocity of flue gas is 12 m/s under

the normal operating conditions. In order to evaluate the effects of inlet velocity of flue gas on the ash particle impaction and distribution along the flue gas flow, five different inlet velocities of 6, 8, 10, 12 and 14 m/s are selected, and they are all in the range of the permitted fluctuation.

Impaction efficiencies of ash particles with diameters of 20 and 0.2 μm in different flue gas velocities are illustrated in Fig. 8(a) and (b) respectively. It is seen in Fig. 8(a) that the impaction efficiency of 20 μm ash particles on the windward sides of heat transfer tubes increases in the first two rows and then decreases gradually in the following rows along the flue gas flow, as numerically simulated in the earlier section. As to the effects of flue gas velocity on the impaction efficiency, it can be found that, impaction efficiency increases with the growth of velocity in the first two rows of the tubes, while in the following tubes along the flue gas flow, the impaction efficiency decreases with increase in the velocity from 8 m/s to 14 m/s. It can be explained by the fact that, as mentioned above, inertial impaction is the most important transport-impaction mechanism for the ash particles. The greater the flue gas velocity is, the more momentum the ash particles have, therefore, the impaction efficiency on the surface of tubes in the first two rows are higher than that in the following rows. For the rest of the rows of tubes, when the flue gas inlet velocity increases from 6 m/s to 8 m/s, although the momentum of ash particles enhances to some extent, they can still follow the flue gas flow; while when the flue gas inlet velocity increases from 8 m/s to 14 m/s, the influence of flue gas flow on motion of the ash particles wanes, thus the ash particles tends to keep their existing trajectories, causing the reduction in the impaction efficiency of ash particles on the surfaces of the heat transfer tubes in the following four rows. As shown in Fig. 8(b), the impaction efficiency of 0.2 μm particles increases slightly with the growth of velocity and tends to form a uniform distribution on both sides of all the heat transfer tube surfaces. The main reason is that, as the inlet velocity increases, the momentum of ash particles also strength. Then they can travel through flue gas barrier to impact on the heat transfer tube surfaces. In addition, the other forces such as Brownian force, Saffman's lift force and thermophoretic force have also pronounced effects on the particle motion, making the ash particles more stochastically distribute on both sides of the heat transfer tubes. Fig. 8(c) indicates the overall impaction efficiency of 20 and 0.2 μm particles on both sides of heat transfer tube surfaces at different inlet velocities. It can be seen that, 20 μm particles have an increase of impaction efficiency with increase of the inlet velocity (from 15.46% at 6 m/s to 24.16% at 14 m/s), while 0.2 μm particles have a gentle impaction efficiency (3.79%-4.62%) at different inlet velocities.

**Effects of longitudinal tube pitch on impaction efficiency:** A dimensionless number $S_1/D$ is used to represent the longitudinal tube pitch. Impaction efficiency of ash particles on the surfaces of heat transfer tube bundle with $S_1/D$ of 1.5, 2, 2.5, 3 and 3.5 are investigated.

Fig. 9(a) and (b) illustrate the impaction efficiencies of 20 and 0.2 μm ash particles on the surfaces of heat transfer tube bundle with different longitudinal tube pitches, respectively. It can be seen from Fig. 9(a), that the impaction efficiency of 20 μm ash particles along the flue gas flow increases in the first two rows, and then decreases in the following rows. However, no significant differences in impaction efficiency are found with the $S_1/D$ increasing from 1.5 to 3.5. According to Fig. 9(b), it indicates that the overall impaction efficiency of 0.2 μm ash particles on the surfaces of heat transfer tubes along the flue gas flow only increases slightly, and there are no obvious differences in the impaction efficiency between the different $S_1/D$. Therefore, it implies that $S_1/D$ has little effect on the impaction efficiency and distribution characteristics along the flue gas flow, which can also be indicated in Fig. 9(c).

**Effects of spanwise tube pitch on impaction efficiency:** A dimensionless number $S_2/D$ is used to represent the spanwise tube pitch. Impaction efficiency of ash particles on the surfaces of heat transfer tube bundle with $S_2/D$ of 1.5, 2, 2.5, 3 and 3.5 are investigated.

Fig. 10(a) and (b) illustrate the impaction efficiencies of 20 and 0.2 μm ash particles on the surfaces of heat transfer tube bundle with different spanwise tube pitches, respectively. It is seen from Fig. 10(a) that, 20 μm ash particles have a relatively high impaction efficiency in the first two rows, and the impaction efficiency on the heat transfer surfaces in the second row is significantly higher than that of all the other rows. In the following rows, the impaction efficiency reduces remarkably, but tends to reach a uniform impaction distribution. As $S_2/D$ increases from 1.5 to 3.5, the impaction efficiency decreases in the first two rows, however, it is found that impaction efficiency increases with an increasing of $S_2/D$ from 1.5 to 3.5 in the third to sixth row. As can be seen in Fig. 10(b), the impaction efficiency of 0.2 μm ash particles show a slightly increase on the surfaces of heat transfer tubes along the flue gas flow. It is also clear that as the impaction efficiency decreases gradually with the increase of $S_2/D$ from 1.5 to 3.5. The main reason is that due to an increase of $S_2/D$ circulation area around the tube bundle increases, which leads to decrease of flue gas and ash particle velocity. The influence of turbulent flow on the ash particle motion is significantly strengthened. More ash particles can be carried by flue gas and travelled downstream with the flue gas. Meanwhile, the degree of turbulent dis-

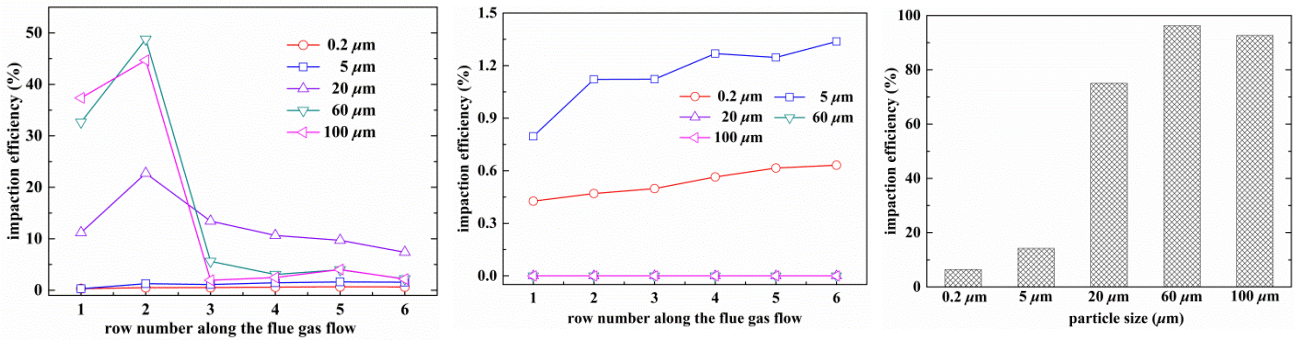


(a) (b) (c)

Fig. 7: Impaction efficiency of ash particles with different sizes: (a) Windward side, (b) Leeward side, (c) Overall impaction efficiency with different particle sizes.

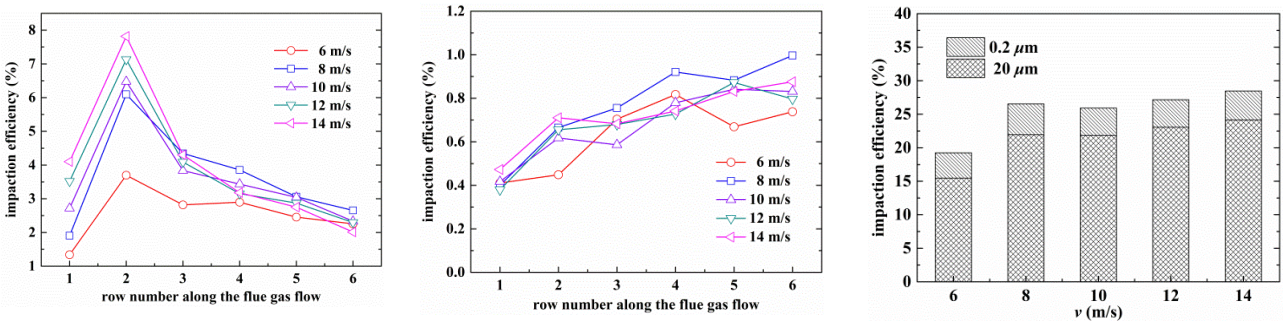


(a) (b) (c)

Fig. 8: Impaction efficiency of ash particles in different flue gas velocities: (a) $d_p$=20 μm, (b) $d_p$=0.2 μm, (c) Overall impaction efficiency at different velocities.

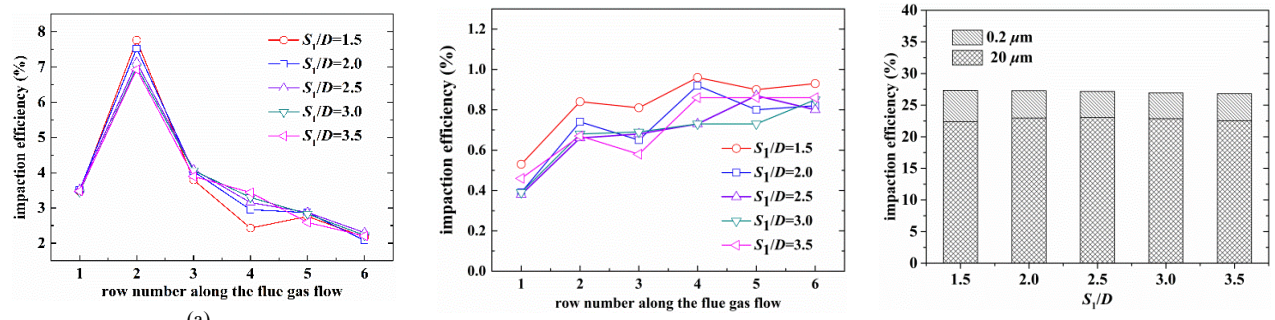


(a) (b) (c)

Fig. 9: Impaction efficiency of ash particles with different longitudinal tube pitches: (a) $d_p$=20 μm, (b) $d_p$=0.2 μm, (c) Overall impaction efficiency at different $S_1/D$.

turbance caused by tube bundle also weakens, then the transverse fluctuation velocity of the flue gas reduces. Therefore, the number of ash particles, especially 20 μm ash particles, captured by the wake vortices decreases obviously. From the above, it can be suggested that the overall impaction efficiency of ash particles with the diameter of 20 and 0.2 μm decreases with an increase of spanwise tube pitch, as shown in Fig. 10(c). When $S_2/D$ is predetermined at 3.5, the overall impaction efficiencies of 20 and 0.2 μm ash particles decreases to 10.89% and 2.12%, which are only 0.35 and 0.18 of the overall impaction efficiencies at $S_2/D$=1.5. The similar tendency of impaction efficiency at different spanwise tube pitches are also found by Han et al. (2014).

## CONCLUSION

A computational model with six-row tube bundle has been

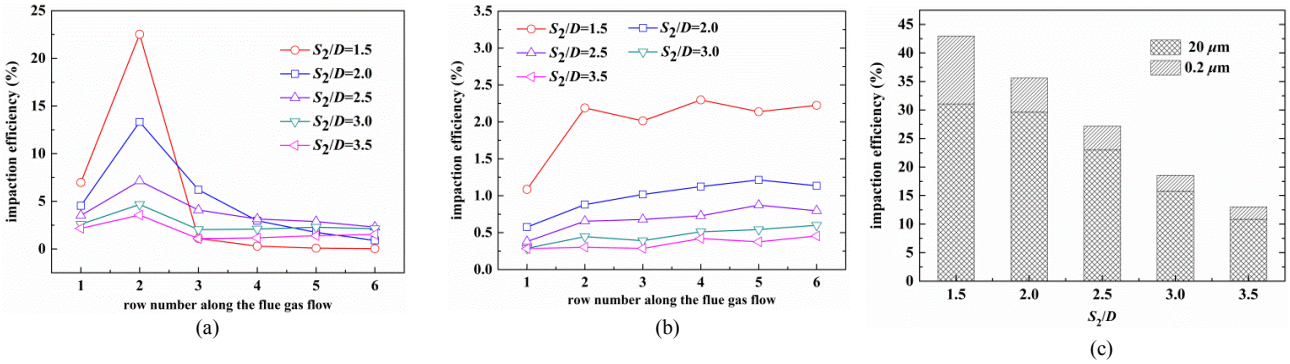


Fig. 10: Impaction efficiency of ash particles with different spanwise tube pitches: (a) $d_p$=20 μm, (b) $d_p$=0.2 μm, (c) Overall impaction efficiency at different $S_2/D$.

carried out to study the gas-particle two-phase flow in the HRSG. The effects of ash particle size, flue gas velocity, longitudinal tube pitch and spanwise tube pitch on ash particle impaction efficiency were investigated numerically. The conclusions obtained as follows:

1. Impaction efficiency increases with the growth of ash particle size. Inertial impaction is the dominant impaction mechanism for large particles, and the results shows that large particles mainly impacts on the windward side of the first two rows with impaction efficiency up to 75% or above. While small particles impact on both windward and leeward sides forming a uniform distribution with impaction efficiency lower than 15%.
2. Enhancing the flue gas velocity contributes more 0.2 and 20 μm ash particles to impact the heat transfer surfaces. Moreover, 20 μm particles were much more sensitive to fluid velocity. Impaction efficiency of 0.2 and 20 μm ash particles increases by 13.7% and 56.3% respectively with the flue gas velocity increasing from 6 m/s to 14 m/s, and the total impaction efficiency increases by 48.0%.
3. The total impaction efficiency shows a slight downward trend with increase of longitudinal tube pitch. The impaction efficiency only decreased by 1.9% with an increase of $S_1/D$ from 1.5 to 3.5. It is thus clear that longitudinal tube pitch has limited effects on ash particle impaction efficiency.
4. Impaction efficiency of ash particles decreases sharply with increase in spanwise tube pitch. Impaction efficiencies of 0.2 and 20 μm ash particles decreases by 82.2% and 64.9% respectively with an increase of $S_2/D$ from 1.5 to 3.5, and the total impaction efficiency decreases by 69.7%. It implies that longitudinal tube pitch plays important role in impaction efficiency of ash particle.

## ACKNOWLEDGEMENTS

This work was financially supported by the National Natural Science Foundation of China (51406025) and the Fundamental Research Funds for the Central Universities (DUT15QY19).

## REFERENCES

Abd-Elhady, M. S., Rindt, C.C.M., Wijers, J. G. and Van Steenhoven, A. A. 2006. Modelling the impaction of a micron particle with a powdery layer. Powder Technol., 168(3): 111-124.

Fang, Q., Wang, H., Wei, Y., Lei, L., Duan, X. and Zhou, H. 2010. Numerical simulations of the slagging characteristics in a down-fired, pulverized-coal boiler furnace. Fuel Process. Technol., 91(1): 88-96.

Guha, A. 2008. Transport and deposition of particles in turbulent and laminar flow. Annu. Rev. Fluid Mech., 40: 311-341.

Han, H., He, Y. L., Tao, W. Q. and Li, Y. S. 2014. A parameter study of tube bundle heat exchangers for fouling rate reduction. Int. J. Heat Mass Tran., 72: 210-221.

Haugen, N.E.L., Kragset, S., Bugge, M., Warnecke, R. and Weghaus, M. 2013. MSWI super heater tube bundle: particle impaction efficiency and size distribution. Fuel Process Technol., 106(2): 416-422.

Lee, B. H., Hwang, M. Y., Seon, C. Y. and Jeon, C. H. 2014. Numerical prediction of characteristics of ash deposition in heavy fuel oil heat recovery steam generator. J. Mech. Sci. Technol., 28(7): 2889-2900.

Li, A. and Ahmadi, G. 1992. Dispersion and deposition of spherical particles from point sources in a turbulent channel flow. Aerosol Sci. Tech., 16(4): 209-226.

Ma, J., Liu, D., Chen, Z. and Chen, X. 2014. Agglomeration characteristics during fluidized bed combustion of salty wastewater. Powder Technol., 253: 537-547.

Mu, L., Zhao, L., Liu, L. and Yin, H. 2012a. Elemental distribution and mineralogical composition of ash deposits in a large-scale wastewater incineration plant: a case study. Ind. Eng. Chem. Res., 51(25): 8684-8694.

Mu, L., Zhao, L. and Yin, H. 2012b. Modelling and measurements of the characteristics of ash deposition and distribution in a HRSG of wastewater incineration plant. Appl. Therm. Eng., 44: 57-68.

Mu, L., Cai, J., Chen, J., Ying, P., Li, A. and Yin, H. 2015. Further study on ash deposits in a large-scale wastewater incineration plant: ash fusion characteristics and kinetics. Energy Fuels, 29(3): 1812-1822.

Pan, Y., Si, F., Xu, Z. and Romero, C. E. 2011. An integrated theoretical fouling model for convective heating surfaces in coal-fired boilers. Powder Technol., 210(2): 150-156.

Sandberg, J., Fdhila, R. B., Dahlquist, E. and Avelin, A. 2011. Dynamic simulation of fouling in a circulating fluidized biomass-fired boiler. Appl. Energ., 88(5): 1813-1824.

Tomeczek, J. and Waclawiak, K. 2009. Two-dimensional modelling of deposits formation on platen superheaters in pulverized coal boilers. Fuel, 88(8): 1466-1471.

Venturini, P., Borello, D., Hanjaliæ, K. and Rispoli, F. 2012. Modelling of particles deposition in an environment relevant to solid fuel boilers. Appl. Therm. Eng., 49: 131-138.

Waclawiak, K. and Kalisz, S. 2012. A practical numerical approach for prediction of particulate fouling in PC boilers. Fuel, 97: 38-48.

Weber, R., Schaffel-Mancini, N., Mancini, M. and Kupka, T. 2013. Fly ash deposition modelling: requirements for accurate predictions of particle impaction on tubes using RANS-based computational fluid dynamics. Fuel, 108: 586-596.

Zbogar, A., Frandsen, F. J., Jensen, P. A. and Glarborg, P. 2005. Heat transfer in ash deposits: A modelling tool-box. Prog. Energ. Combust., 31(5): 371-421.

Zbogar, A., Frandsen, F., Jensen, P. A. and Glarborg, P. 2009. Shedding of ash deposits. Prog. Energ. Combust., 35(1): 31-56.

Zhou, H., Jensen, P. A. and Frandsen, F. J. 2007. Dynamic mechanistic model of superheater deposit growth and shedding in a biomass fired grate boiler. Fuel, 86(10): 1519-1533.

Zukauskas, A. 1987. Heat transfer from tubes in cross-flow. Adv. Heat Tran., 18: 87-159.